doi:10.1038/nature12131

S1 Calculating the static contribution to J_4

To determine the largest possible range of $J_4^{\rm static}$ values we use a suite of core/envelope internal structure models, with a wide range of core depths, core densities and envelope density profiles. The core is taken to be of constant density with the core density ranging between $0.8\times10^4 < \rho_{\rm core} < 1.2\times10^4$ kg m^{-3}, and core radius extending up to 30% of the planetary radius on Neptune ($0 < r_{\rm core} < 0.3\,R$, where R is the mean planetary radius), and 20% on Uranus, following the widest possible range of core densities given by [16, 17, 19]. We systematically explore this parameter space where for each case of $\rho_{\rm core}$ and $r_{\rm core}$ we then match an envelope represented by a 6th order polynomial with a monotonic density distribution so that

$$\rho_{\rm static} = \rho_{\rm core} \quad \text{for} \quad 0 < r < r_{core} \tag{S1}$$

$$\rho_{\rm static} = a_0 + a_2\beta^2 + a_3\beta^3 + a_4\beta^4 + a_5\beta^5 + a_6\beta^6 \quad \text{for} \quad r_{\rm core} < r < R, \tag{S2}$$

where $\beta = r/R$ is the normalized radius. The coefficients (a_n) are determined by constraints on the static density ($\rho_{\rm static}$). The first constraint on the static density is that the density is zero at the surface, satisfied by setting the sum of the six polynomial coefficients to zero at $\beta = 1$. The second constraint is that the integrated density over the entire volume must equal to the planetary mass. The third constraint is that the density derivative at $\beta = 1$ equals the derivative of the density at the 1 bar pressure level (equal to -0.1492 and -0.2425 kg m^{-4} for Uranus and Neptune respectively, [31]). The first degree term in Eq. S2 is missing so that the derivative of the density goes to zero at the center for models with no core, and another constraint sets this value to zero at the core-envelope boundary for models with cores. The last constraint limits the value of J_2 to within the error estimates of the observed value of $3341.29\pm0.72\times10^{-6}$ and $3408.43\pm4.50\times10^{-6}$ for Uranus and Neptune respectively [14, 15]. Since we are interested in determining the resulting J_4 we do not impose any constraints on J_4, as done in most studies where the J_4 is constrained to

within the observed values of J_4 (e.g., [13]). For cases with no core the density at $\beta = 0$ is not constrained, and its derivative at $\beta = 0$ is set to zero.

	Uranus	Neptune
Mass [$\times 10^{25}$ kg]	8.681	10.241
Rotation period (Voyager values) [hour]	-17.24	16.11
Equatorial radius [km]	25559 ± 4	24764 ± 15
Polar radius [km]	24973 ± 20	24341 ± 30
Mean radius [km]	25362 ± 7	24622 ± 19
RMS deviation from spheroid [km]	16.8	8
q	0.0261	0.0295
Surface equatorial gravity [m s^{-2}]	8.87	11.15
$J_2 \times 10^6$ (observed)	3341.29 ± 0.72	3408.43 ± 4.50
$J_4 \times 10^6$ (observed)	-30.44 ± 1.02	-33.40 ± 2.90

Table S1: Uranus and Neptune planet characteristics [32, 14, 15, 33]. The gravity field values correspond to a reference equatorial radius of 26,200 km for Uranus and 25,225 km for Neptune following the convention in [32]. (In the literature these values often appear corresponding to different reference radii, and to normalize them they need to be multiplied by a normalization factor given by the reference radius ratio to the harmonic power [25].)

The value of J_2 and J_4 are determined using third order theory of figures [12], in which J_2 and J_4 are expanded to third order in the small rotational parameter. The small rotational parameter $q = \frac{\Omega^2 R^3}{GM}$ is a dimensionless parameter given by the rotation rate Ω, the equatorial radius R, the mass M and the gravitational constant $G = 6.67 \times 10^{-11}$ m^3 kg^{-1} s^{-2}. The q values for Uranus and Neptune are given in Table S1. The harmonics are expanded as $J_{2n} = \Sigma \Lambda_{2n} q^n$ to third order in q, where the coefficients Λ_{2n} are determined by the shape and radial distribution of the density given by the coefficients a_n. To leading order $J_2 = \Lambda_2 q$, where the smaller the value of Λ_2 the more centrally condensed is the mass of the planet. For a constant density Maclaurin spheroid, this value will be $\Lambda = 0.5$, and for any compressible fluid, as in the case of the density profiles we use here, $\Lambda_2 < 0.5$ [11, 34]. Thus for every set of coefficients (a_n), the density profile gives a specific J_4 and J_2 based on the theory of figures, which accounts for the planet's geopotential shape (oblateness) and interior mass distribution. Lower order polynomials (4th and 5th order) give similar results for the derived J_2 and J_4. For each model we begin with an initial guess for the density profile and then

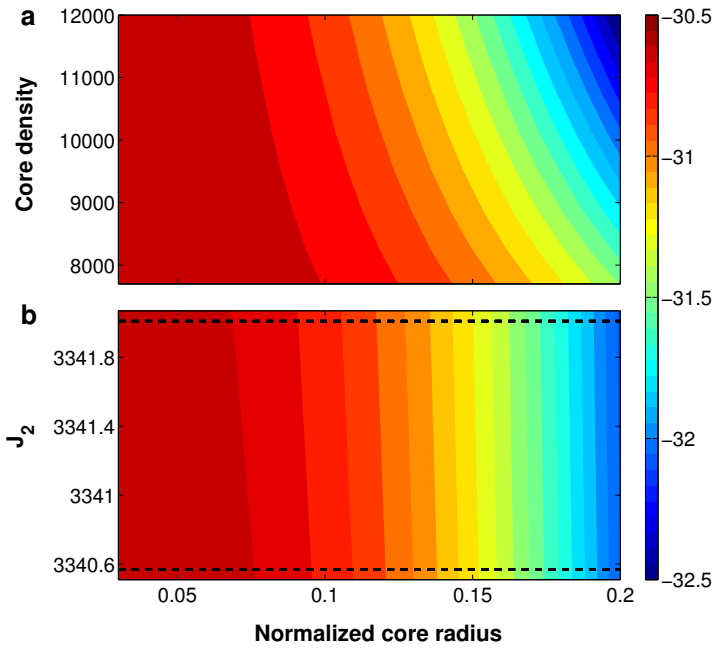

Figure S1: $\mathbf{J_4^{static}\left(\times 10^6\right)}$ **over a wide range of interior models for Uranus. a**, J_4^{static} as function of normalized core radius and core density (kg m^{-3}) with J_2 held constant at the mean observed value of $J_2 = 3341.29 \times 10^{-6}$ [14]. **b**, J_4^{static} as function of normalized core radius and $J_2\left(\times 10^6\right)$ with the core density set to 1.01×10^4 kg m^{-3}, and $J_2 = 3341.29 \pm 0.72 \times 10^{-6}$ varying between the observed uncertainty (dashed lines).

evaluate J_2. The difference between the calculated J_2 and the observed value is used to correct the density function, and the process is iterated to convergence (e.g., [13, 35]).

The objective of this analysis is to cover the widest possible range of interior solutions. This results in a conservative estimate for the difference between the observed J_4 and J_4^{static}, which is the dynamical contribution to J_4. Due to the uncertainty in the core mass, core radius and the exact observed value of J_2 we consider a wide range of interior models where we systematically vary these parameters within the broadest range of reasonable values. The core density is varied in increments of 800 kg m^{-3} between the values discussed above, the core radius in increments of $0.01R$, and J_2 in increments of 9.4×10^{-8} and 4.3×10^{-7} for Uranus and Neptune respectively. Models with no cores are considered as well. Thus we consider an ensemble of about 3000 different interior models for Neptune and 1500 for Uranus. For each of these models for ρ_{static} we

repeat the calculation of $J_4^{\rm dyn}$ described in detail in section S2. The fact that the density profile is represented by a fitted polynomial and not calculated by an equation of state may lead to that some of these profiles are unrealistic in the sense that they do not reproduce the behavior of high pressure hydrogen/helium/ices/rocks. However, for the goal of giving an upper bound to the depth of the dynamics we chose using a broad range of $\rho_{\rm static}$ solutions, and this analysis would not have been possible if using only the few existing profiles based on suggested equation of states (e.g., 16, 6, 19). Nevertheless, we have also repeated our analysis with physically based $\rho_{\rm static}(r)$ profiles (those of Hubbard 1989, Hubbard 1991 and Nettelmann 2012, [16, 6, 19]), where $\rho_{\rm static}(r)$ is obtained by three layer models including a molecular envelope, an icy intermediate layer, and a rocky core, and find that these also give results for the dynamical response of $\Delta J_4^{\rm dyn}$ that fall within the range of solutions in Fig. 4. Therefore we conclude that since our interior models cover a large and inclusive parameter space of solutions, our estimates for the penetration depth of the winds can be considered to be conservative, although it is still possible that future new, more sophisticated interior structures will lead to slightly different values of J_{2n}.

S2 Calculating the dynamical contribution to J_4

Uranus and Neptune's rapid planetary rotation and large scale fluid motion (thus small Rossby numbers) put them in a dynamical regime where their total angular momentum $M \equiv M_\Omega + M_u = \Omega r^2 \cos^2\theta + ur\cos\theta$ is dominated by the planetary rotation (first term), where Ω is the planetary rotation rate, u is the azimuthal (zonal) relative wind velocity and θ is latitude. This implies that to leading order surfaces of constant angular momentum per unit mass are aligned in the direction of the axis of rotation [36, 20, 21], approximately as cylinders parallel to the rotation axis. Conservation of angular momentum then implies that convective fluid motion in the interior flows along these surfaces [37, 36, 20], so that $\mathbf{u}\cdot\nabla M_\Omega = 0$ ($\mathbf{u}$ is the 3D wind vector) [21], meaning that to leading order there can be no flow through surfaces which are parallel to the axis of rotation [36, 20, 21]. In the purely barotropic limit this will imply a Taylor-Proudman state, namely that

the velocity must be constant along the direction of the axis of rotation [23]. However meridional entropy gradients due to internal or solar heating (on Neptune internal hating is stronger than the incoming solar heating, while on Uranus the internal heating is very small) can drive these systems away from the barotropic state, resulting in zonal wind shear along the direction of the axis of rotation [20]. The magnitude of this shear will then depend on the details of the interior thermodynamics [36, 20]. In addition, the magnetic field can cause a weaker interior flow due to ohmic dissipation [22]. Therefore only flow along (not across) surfaces parallel to the spin axis can exist, but the zonal wind can have shear along the direction of the spin axis. Given these constraints on the zonal wind, we define a general dynamical state for the zonal wind $u(r,\theta)$ with equilibrium winds that depend both on latitude (θ) and radius (r). For this general wind profile we use a free parameter H so that the wind profile is defined as

$$u(r,\theta) = u_0 e^{\left(\frac{r-a}{H}\right)}, \tag{S3}$$

where H is an e-folding decay depth of the cloud level winds representing the zonal wind shear, and $u_0(r,\theta)$ are the observed cloud level zonal winds extended constantly along the direction of the axis of rotation defined as

$$u_0(r,\theta) = u_{cl}\left[\arctan\left(\frac{\sqrt{R^2 - r^2\cos^2\theta}}{r\cos\theta}\right)\right], \tag{S4}$$

where $u_{cl}(\theta)$ are the observed cloud level winds [38]. Varying systematically the free parameter H gives a continuous set of wind profiles, which depend on one parameter that allows us to explore the dynamic gravity harmonics resulting from the wind. When H is small the winds are confined to a shallow layer, and when H is large the winds approach the barotropic state where the winds penetrate through the planet along the direction of the spin axis (this state where H is large is similar to what is often referred to as differential rotation). Thus, the choice of the exponential decay along angular momentum surfaces, which is based on the vertical profile of the entropy expansion coefficient that controls the baroclinic shear in 3D anelastic general circulation models [36, 20],

and the decay of interior flow due to MHD Ohmic dissipation effects [22], allows exploring the full range of wind profiles from deeply rooted winds extending throughout the planet to shallow surface winds. The wind profile is then used to calculate the density anomaly gradients balancing this circulation.

To calculate the density anomaly resulting from this zonal velocity we consider the momentum equations for a rotating invicsid fluid given by

$$\frac{\partial \mathbf{u}}{\partial t} + (2\Omega + \omega) \times \mathbf{u} = -\frac{1}{\rho}\nabla p - \mathbf{g} - \nabla \frac{1}{2}\mathbf{u}^2, \tag{S5}$$

where ω is the vorticity vector ($\omega = \nabla \times \mathbf{u}$), Ω is the planetary rotation vector, $\mathbf{g}$ is the gravitational acceleration, and p and ρ are the pressure and density fields respectively [23]. Taking the curl of (S5) multiplied by the density ρ gives for small Rossby numbers in a statistical steady state

$$2\Omega\nabla \cdot (\rho \mathbf{u}) - 2\Omega \cdot \nabla (\rho \mathbf{u}) = -\nabla\rho \times \mathbf{g}. \tag{S6}$$

We expand the density and pressure as a basic hydrostatic state and a perturbation due to the dynamics

$$\rho = \rho_{\text{static}}(r) + \rho'(\phi, \theta, r, t) \tag{S7}$$

$$p = p_{\text{static}}(r) + p'(\phi, \theta, r, t), \tag{S8}$$

where the hydrostatic state is

$$\frac{\partial p_{\text{static}}}{\partial r} = -\rho_{\text{static}} g, \tag{S9}$$

and $\rho' \ll \rho_{\text{static}}$. Here we have assumed spherical geometry, such that the gravity $g(r)$ has only a radial component (for a deep atmosphere the gravity will vary with depth), and the variables

ρ_{static} and p_{static} are functions only of r. This is justified by the fact that the dynamics are a perturbation to the mean hydrostatic state, and the planet's deviation from spherical geometry is small (the equatorial radius is larger than the polar radius by 2.3% and 1.7% for Uranus and Neptune respectively [33]), and therefore we can to good approximation calculate the dynamical contribution to the gravity harmonics (ΔJ_n^{dyn}) in spherical geometry. This approximation retains density anomalies ρ' associated with the velocity field $\mathbf{u}$, but does not retain the dynamical density distortions associated with overall planetary oblateness which we discuss in detail below. Then, using the continuity equation the vorticity equation (S6) becomes

$$2\Omega \cdot \nabla \left(\rho_{\text{static}} \mathbf{u}\right) = \nabla \rho' \times \mathbf{g}, \tag{S10}$$

giving a general form of the thermal wind balance without any assumptions about the depth of the atmosphere (thus without the traditional approximation where the vertical Coriolis terms are neglected). This gives a relation between the dynamical density gradient and the velocity field. Since we seek to relate only the zonal component of the wind $u(r,\theta)$, to the dynamical density perturbations we consider next only the zonal component of (S10), thus

$$2\Omega \left[\frac{\partial \left(\rho_{\text{static}} u\right)}{\partial r} \sin\theta + \frac{\rho_{\text{static}}}{r} \frac{\partial u}{\partial \theta} \cos\theta \right] = \frac{1}{r} \frac{\partial \rho'}{\partial \theta} g, \tag{S11}$$

where the gradient in the direction of the axis of rotation has been split into its radial and latitudinal components. We integrate (S11) over latitude to obtain an expression for the density anomaly

$$\rho'(r,\theta) = \int_{-\frac{\pi}{2}}^{\theta} \frac{2\Omega}{g} \left[\frac{\partial \left(\rho_{\text{static}} u\right)}{\partial r} \sin\theta' + \frac{\rho_{\text{static}}}{r} \frac{\partial u}{\partial \theta'} \cos\theta' \right] r d\theta' + \rho_0'(r), \tag{S12}$$

where ρ_0' is an integration constant and therefore only a function of radius.

This density anomaly (ρ') will contribute a dynamical contribution to the gravity harmonics

defined as

$$\Delta J_n^{\rm dyn} = -\frac{1}{Ma^n}\int_0^a r'^{n+2}dr'\int_0^{2\pi}d\phi'\int_{-1}^{1}P_n\left(\mu'\right)\rho'\left(r',\mu'\right)d\mu', \tag{S13}$$

where ϕ is longitude, P_n is the n-th Legendre polynomial and $\mu = \cos\theta$. Since we have considered the dynamics in hemispherical symmetry, where the wind profile $u_0(r,\theta)$ is an average of the winds in the northern and southern hemisphere, the odd harmonics are zero. Since the wind profile is nearly hemispherically symmetric (Fig. 1), using only the northern (or southern) hemisphere wind profile, rather than their average, makes very small difference to the results. The contribution of $\Delta J_2^{\rm dyn}$ is small compared to the difference between the observed J_2 and $J_2^{\rm static}$ and therefore will not give any constraints on the depth of the flow. However, due to the latitudinal structure of the zonal winds and the smaller values of the observed J_4 and $J_4^{\rm static}$, the dynamical contribution to J_4 ($\Delta J_4^{\rm dyn}$) is large enough to be equivalent in magnitude to the difference between the observed J_4 and $J_4^{\rm static}$. Thus estimating $\Delta J_4^{\rm dyn}$ as function of the decay scale H and comparing it to $J_4^{\rm observed} - J_4^{\rm static}$ will provide constraints on the depth of the circulation which is the objective of this paper.

For every interior density profile $\rho_{\rm static}$ and H we can determine ρ' up to the integration constant $\rho_0'(r)$, which cannot be determined uniquely. Note that ρ_0' is a function of r alone. Then plugging Eq. (S12) into Eq. (S13) allows us to calculate $\Delta J_4^{\rm dyn}$. Under the assumption that ρ' is computed in spherical geometry, $\rho_0'(r)$ has no projection onto Legendre polynomials and therefore no contribution to $\Delta J_4^{\rm dyn}$. Nonetheless, if projected onto the oblate spheroid $\rho_0'(r)$ could contribute in a manner analogous to $\rho_{\rm static}$ (which is also a function of radius), and this implies that ρ_0' can potentially provide a dynamical contribution to $\Delta J_4^{\rm dyn}$ due to the oblateness of the planet.

However, this contribution is sufficiently small that it is negligible compared to the contribution of $\rho_{\rm static}$. The basic-state profile $\rho_{\rm static}(r)$ represents the density of a wind-free, static interior, and $\rho_0'(r)$ represents a perturbation to the horizontal-mean radial density profile (if any) *due to dynamics*. Note that dynamics is not generally the source of buoyancy perturbations in an atmosphere or interior; rather, the fundamental role of dynamics is simply to *rearrange* buoyancy and entropy

perturbations produced by some independent mechanism (radiation, latent heating, etc). This argues that, to order of magnitude, the density perturbations ρ_0' are comparable to (or less than) the horizontal density perturbations associated with the thermal-wind shear (i.e., the second term in Eq. (S12) should not greatly exceed the first term). In addition, since the first term in Eq. (S12) is a function of both radius and latitude and the second term a function of only radius it is impossible that both terms are significantly larger than their sum ρ'. To estimate the ratio of the dynamical to static density terms we note that for a geostrophic flow the fractional horizontal density perturbations (i.e., the ratio of the first term in Eq. (S12) to $\rho_{\rm static}$) are $O(\frac{\Omega u L}{gH})$, where L is a typical length scale of the motion, u is the typical zonal velocity, and H is the scale height of the flow [23]. Taking $L = 10^4\,$km, $u = 200\,{\rm m\,s^{-1}}$, and $H = 1000\,$km gives a ratio of $\sim$2% for both Uranus and Neptune. Therefore this implies that the perturbation to $\Delta J_4^{\rm dyn}$ caused by ρ_0' is at most $\sim$2% of $J_4^{\rm static}$. Since $J_4 \sim -30\times10^{-6}$ for both planets, the perturbation to J_4 due to $\rho_0'(r)$ is $\sim 0.6\times10^{-6}$ or less. This perturbation is an order of magnitude smaller than the difference between the observed J_4 and $J_4^{\rm static}$ and thus this source of uncertainty has a negligible effect on our analysis and results. Similarly, Kong et al. [9], who estimate the dynamical contribution of the low harmonics on Jupiter using a fully oblate spheroid model, find that they are of order of less than 1% than that of the solid body part for J_2 and J_4. Note that for the case of Uranus and Neptune due to the particular latitudinal structure of the winds, the winds have a large projection on P_4, and therefore the dynamical effect on the harmonics becomes amplified. This leads to the fact that for deep H cases the dynamical effect of the *latitudinally* varying part of Eq. (S12) is comparable in magnitude to that of $\rho_{\rm static}$ even though the ratio of $\rho'/\rho_{\rm static}$ is small, while the dynamical contribution to J_4 of the non-latitudinally varying part (ρ_0') will be no more than the ratio of $\rho'/\rho_{\rm static}$.

Note that, formally, it would be possible to rework our analysis by identifying the basic-state, radially varying density profiles $\rho_{\rm basic-state}(r)$ used in interior models (cf Eq. (S1) – (S2) and Figs. 2–3) not with $\rho_{\rm static}$, as we have done, but with the sum of $\rho_{\rm static}(r)+\rho_0'(r)$. A key point is that the density profiles shown in Fig. 3 and described in Section S1 do not make any dynamical assumptions (for example, they do not assume an isentropic interior) nor do they assume any

specific equations of state for plausible interior materials. As a result, our interior models make no assumption that the interior lacks any horizontally averaged dynamical density perturbations. It is perfectly possible that some portion of the radial density profile $\rho_{\mathrm{basic-state}}(r)$ represented by Eq. (S1) – (S2) might result from horizontally averaged, radially varying dynamical perturbations to the static, wind-free density structure. In constructing our ensemble of interior models for each planet, the mathematical statement that we vary a_0 to a_6 (and other parameters) over a wide range would then be equivalent to the physical statement that we are varying the *sum* of the interior static, wind-free structure and the horizontally-averaged, dynamically-induced density profiles over a wide range. In this approach, $\rho_0'(r)$ would not appear in Eq. (S12) since it is already included in $\rho_{\mathrm{basic-state}}(r)$; the J_4^{static} values calculated in our paper then already include the effect of ρ_0', and all the constraints on the depth of the winds on Uranus and Neptune follow exactly as described in the paper.

The dynamical model is based on the fact that to leading order the planet is geostrophically balanced, which results in the cylindrical symmetry manifested in the choice of the velocity structure (Eq. S3). This relies on the Rossby number being much less than one, which is known given the planet's wind speeds, length scales, and planetary rotation rate. Moreover, cloud tracking observations demonstrate that the zonal-mean component of the flow greatly exceeds the eddy velocities. These facts motivate a model adopting geostrophy and zonal symmetry of the winds. It is possible to envision scenarios where H varies in latitude (if there are latitudinal internal structure differences that affect the decay depth). In that case, the present analysis constrains the long-wavelength component of H to be less than $\sim 10^3$ km. This does not rule out the possible existence of small-scale, locally confined latitude regions where H exceeds these limits. But the latitudinally averaged H must be smaller than the limits described here. A possible exception is an interior zonal wind with an opposite sign to the upper winds, which compensates for the J_4 signature of the outer winds. However, such a flow is unphysical (due to both compressibility and MHD effects discussed previously), and there has been no suggested physical mechanisms or model that would cause the interior flow to switch sign.

The confinement of the jets to a shallow layer implies that the dynamics are likely driven shallow processes, rather than from deep columnar structures that penetrate through the planet (e.g., 4, 37). Yet, internal convective heating may still be significant in driving the jets. Thermal wind balance implies that decay of the fast surface winds to small values within a shallow layer requires large horizontal density contrasts on isobars in the deep atmosphere. These could plausibly be provided by latent heating due to condensation of water at pressures of ~ 300 bars [2]. Note that, although such latent heating occurs at depths shallow compared to the planet as a whole, sunlight penetrates to pressures of only a few bars, and thus such latent heat release is nevertheless associated with the loss of internal heat from the planetary interior. Although the winds themselves are confined to a layer potentially extending to thousands of bars, it is also possible that the eddy-momentum convergences that drive those jets extend only a fraction of the way through that layer [39, 40, 21, 3]. Thus despite the jets being shallow compared to the planetary radii and involve only a small fraction of the planetary mass, our depth constraint does not imply necessarily on the driving mechanism of the jets.

In summary, in this analysis for every interior density profile ($\rho_{\rm static}$) discussed in section S1, and zonal wind velocity decay scale (H) ranging from 10 km to 10^5 km, we calculate the gravity harmonics due to dynamics ($\Delta J_4^{\rm dyn}$) based on Eq. (S13) using the dynamical density given by Eq. (S12). Fig. 4 shows the resulting $\Delta J_4^{\rm dyn}$ solution limits as function of H, where all solutions for the ensemble of interior structure models discussed in section S1, and three layer interior models [16, 6, 19], are in between the two blue lines. Particularly, using the three layer model profiles from [6] gives a maximum H of $H = 1040$ km and $H = 970$ km for Uranus and Neptune respectively and when using profiles N1 and U1 from [19] $H = 880$ km and $H = 830$ km for Uranus and Neptune respectively. Therefore we find that the *maximum* depth of the winds that will give a small enough dynamical gravity harmonic $\Delta J_4^{\rm dyn}$, can be only $\sim 1,100$ km on Uranus and Neptune, which are equivalent to a depth containing only the outermost 0.15% of the mass (roughly 2000 bars) and 0.2% of the mass (roughly 4000 bars) on the two planets respectively.

References

[31] Lodders, K. & Fegley, B. *The planetary scientist's companion* (1998).

[32] JPL's Solar System Dynamics Group. JPL database. Http://ssd.jpl.nasa.gov.

[33] Seidelmann, P. K. et al. Report of the IAU/IAG Working Group on cartographic coordinates and rotational elements: 2006. *Celestial Mechanics and Dynamical Astronomy* **98**, 155–180 (2007).

[34] Hubbard,W. B. High-precision Maclaurin-based models of rotating liquid planets. *Astrophys. J. Let.* **756**, L15 (2012).

[35] Helled, R., Anderson, J. D., Schubert, G. & Stevenson, D. J. Jupiter's moment of inertia: A possible determination by Juno. *Icarus* **216**, 440–448 (2011).

[36] Kaspi, Y. *Turbulent Convection in Rotating Anelastic Spheres: A Model for the Circulation on the Giant Planets.* Ph.D. thesis, Massachusetts Institute of Technology (2008).

[37] Busse, F. H. A simple model of convection in the Jovian atmosphere. *Icarus* **29**, 255–260 (1976).

[38] Porco, C. C. et al. Cassini imaging of Jupiter's atmosphere, satellites and rings. *Science* **299**, 1541–1547 (2003).

[39] Showman, A. P., Gierasch, P. J. & Lian, Y. Deep zonal winds can result from shallow driving in a giant-planet atmosphere. Icarus **182**, 513–526 (2006).

[40] Lian, Y. & Showman, A. P. Deep jets on gas-giant planets. Icarus **194**, 597–615 (2008).